Jurnal Teknologi

Full Paper

THE SIMULATION OF INTERMOLECULAR INTERACTIONS OF CARBOXYLIC AND AMINE GROUPS WITH CALCIUM CARBONATE

Abu Zar Che Azimi[a], Norhayati Abdullah[a]*, Fatmawati Adam[a], Zulkafli Hassan[a], Sunarti Abdul Rahman[a], Mohd Zulhaizan Mohd Noor[b]

[a]Faculty of Chemical and Process Engineering Technology, Universiti Malaysia Pahang, Lebuh Persiaran Tun Khalil Yaakob, 26300 Kuantan, Pahang, Malaysia
[b]Setegap Ventures Petroleum Sdn. Bhd., No. 68 & 70 Fraser Business Park, Jalan Metro Pudu 2, 55200 Kuala Lumpur, Malaysia

Article history
Received
29 April 2022
Received in revised form
11 October 2022
Accepted
20 October 2022
Published Online
26 December 2022

*Corresponding author
yatiabdullah@ump.edu.my

Graphical abstract

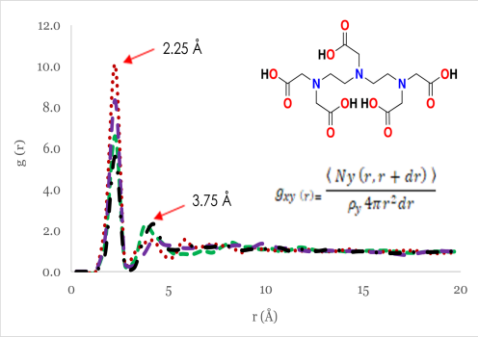

Abstract

Surface facilities including tubing and valves at the oilfield have been plagued by mineral scale deposits, which are constitute of calcium carbonate ($CaCO_3$). Penta-potassium diethylenetriaminepentaacetic acid salt (DTPA-K_5) has a higher affinity for the metal cations complexes during the chelation process. The eight complexing sites (five carboxylate and three amines) empower the metal ion interactions. This work investigated the molecular dynamics simulations between the DTPA-K_5 with the calcium carbonate, $CaCO_3$ scale. The interaction was performed through molecular dynamic (MD) simulation using condensed phase optimised molecular potentials for atomistic simulation studies (COMPASS) force field and the Ewald summation method in Material Studio. The simulation trajectory files examined the intermolecular interactions for radial distribution function (RDF). The simulation shows strong DTPA-K_5 with calcium interactions, which revealed the metal ion complexes contributing to the chelation process through the reactive carboxylic and amine functional groups, which were O_7 == Ca at radius, r, 2.25 Å with g(r) of 10.09 and N_1 -- Ca at radius, r, 2.25 Å with g(r) 2.51.

Keywords: Chelating agent, COMPASS, molecular dynamic simulation, calcium carbonate, radial distribution function

Abstrak

Kemudahan permukaan termasuk tiub dan injap di medan minyak telah dibelenggu oleh mendapan skala mineral, yang merupakan kalsium karbonat ($CaCO_3$). Garam asid penta-kalium diethylenetriaminepentaacetic (DTPA-K_5) mempunyai pertalian yang lebih tinggi untuk kompleks kation logam semasa proses pengkelatan. Lapan tapak kompleks (lima karboksilat dan tiga amina) memperkasakan interaksi ion logam. Kerja ini menyiasat simulasi dinamik molekul antara DTPA-K_5 dengan kalsium karbonat, skala $CaCO_3$. Interaksi dilakukan melalui simulasi dinamik molekul (MD) menggunakan potensi molekul dioptimumkan fasa terkondensasi untuk medan daya kajian simulasi atom (COMPASS) dan kaedah penjumlahan Ewald dalam Material Studio. Fail trajektori simulasi memeriksa interaksi antara molekul untuk fungsi pengedaran jejari (RDF). Simulasi menunjukkan DTPA-K_5 yang kuat dengan interaksi kalsium, yang mendedahkan kompleks ion logam yang menyumbang kepada proses

pengkelatan melalui kumpulan berfungsi karboksilik dan amina reaktif, iaitu O_7 == Ca pada jejari, r, 2.25 Å dengan g(r) sebanyak 10.09 dan N_1 -- Ca pada jejari, r, 2.25 Å dengan g(r) 2.51.

Kata kunci: Agen pengkelatan, COMPASS, simulasi dinamik molekul, kalsium karbonat, fungsi taburan jejari

1.0 INTRODUCTION

Chemical scale accumulation of insoluble mineral salts on water pipeline equipment is a significant problem in the oil field. The mineral deposits can be barium sulfate, calcium carbonate, calcium sulfate, iron sulfide and strontium sulfate contributing to faults inflow restriction, equipment wear, costly repair, and maintenance interruptions, thus decreasing the efficiency of chemical processing production [1, 2].

In oilfield chemical treatments, chelating agents are chemicals used to regulate uncontrolled metal ion reactions from recombination and lead to precipitation [3,4]. Ethylenediaminetetraacetic acid (EDTA) and glutamic acid diacetic acid (GLDA)] have replaced conventional acids, such as hydrochloric acid (HCl), hydrofluoric acid (HF), and organic acids, at high temperature and salinity conditions to stimulate carbonate and sandstone reservoirs without any side effects on the formation integrity. Diethylenetriaminepentaacetic acid (DTPA) and GLDA are effective in removing different types of scales, such as carbonate, sulfate, and sulfides and have the advantages for not releasing hydrogen sulfide (H_2S) and using corrosion inhibitors [5]. Penta-potassium salt diethylenetriaminepentaacetic acid (DTPA-K_5) is a polyaminocarboxylic acid (PACA) with five carboxylic groups and three amines chelating agents used for removing different types of solid scale in the petroleum industry application [6, 7]. The scale-dissolution activity necessitates creating complex formations with metal ions to obtain water-soluble and reasonably stable combinations. DTPA was formulated in the addition of oxalic acid, tannic acid, non-ionic surfactant, and water as a dissolver for real barium scale sample demonstrated efficiency of 71-77% at 35°C and 78-91% at 90°C dissolution efficiency, respectively [8]. A study highlighted the best condition for the $BaSO_4$ scale to dissolve was at 80°C and a longer contact time of 48 hours to prolong the dissolution time of the solid scale [9]. 20 wt.% of DTPA and 6 wt.% potassium carbonates, K_2CO_3 are exposed to both $CaCO_3$ and $BaSO_4$ scales. The affinity result of DTPA is higher to calcium compared to barium which solubility of $BaSO_4$ is getting low in DTPA and K_2CO_3 in comparison to $CaCO_3$ [10].

In a real scale sample calcium (Ca^{2+}) was detected in the precipitated silica sand from oil well. Other chemical elements such Al, Fe and O also were detected [11]. This suggests the complexity of metal elements formed in the solid scale of an oil well. This is one motivation for this work to understand the knowledge gap of chelating agents that would interact with $CaCO_3$ solid scale at molecular scale as one of the most chemical elements present in oil well scale.

The functional groups play a vital role by enabling circular free metal ion interaction (chelation), forming a high stability ring-like structure [12]. These ligands were deprotonated at the highest pH values using hydroxide salt and water [13, 14]. Glutamic acid hydrochloride, which is water-soluble, can dissolve $CaCO_3$ at around 3000 ppm [15]. A molecular dynamic study demonstrated that carboxylic group formed a strong intermolecular interaction with Ca^{2+} and Fe^{2+} metal ions at 2.25 Å [16].

Understanding how functional group-promoting at the molecular level mechanisms is essential for the DTPA-K_5 solvent dissolution of solid scale application. Simulation study demonstrated that OH from the carboxylic group has a stronger intermolecular interaction between calcium ions and Glutamic acid diacetate (GLDA) at the nanoscale level to understand the solid scale dissolution in the oilfield [16]. Furthermore, the radial distribution function of patchouli solute in different polar and nonpolar solvents reflects the dissolution of patchouli in the extraction process [17]. This work investigated the interactions between the DTPA-K_5 with calcium carbonate using molecular dynamic (MD) simulations. The findings may suggest better dissolver formulations in developing new solid scale removal, thus enhancing the dissolution.

2.0 METHODOLOGY

2.1 Molecular Dynamic Simulation

Computational chemistry studies of complexation metal ions were conducted using the molecular dynamics simulation technique in Acceryls Materials Studio Studio (MS) version 5.5 program. Initially, the 3D molecular structure of DTPA-K_5, $CaCO_3$, and H_2O was downloaded from ChemSpider online databases. Figure 1 illustrates the chemical structure of the DTPA, DTPA-K_5, and $CaCO_3$ molecules, which were labelled accordingly. The carboxyl groups of DTPA were labelled with numbers 1 to 5 and DTPA-K_5 with numbers 6 to 10. The hydroxyl group's single

bond is indicated by the dash character (--), while the carbonyl group's double bond is expressed by the equal sign (==). Initially, geometry optimisation and energy minimisation step were made based on a smart minimiser operating in fine quality mode. Next, the cubical simulation model was configured and completed using the amorphous cell module for each system with a minimum energy level [18]. Figure 2 shows a cubical simulation model comprised of DTPA-K_5, $CaCO_3$ and water molecules. Subsequently, the simulation started at 1000 ps for each NVE (constant number of atoms, volume, energy) and NPT (constant number of atoms, pressure, and temperature) thermodynamic ensembles. A 1.0 fs time step was set throughout the calculation. The intermolecular interactions were simulated at 333.15 K and 136 atm using the third-generation force fields COMPASS and the Ewald-based summation technique for calculation of non-bonding van der Waals force and electrostatic interactions with a precision of 0.0001 kcal/mol [19, 20, 21, 22, 23]. The COMPASS force field potentially simulates organic molecules, inorganic gases, and polymers. A review of the simulation system is presented in Tables 1. System 1 represents DTPA in water and system 2 represents the $CaCO_3$ scale in DTPA and water. Meanwhile, system 3 and system 4 considered the improvement of DTPA structure with potassium (K). The radial distribution function (RDF) between each atom or molecule was evaluated at the end of the simulation. These RDFs value g(r) highlighted the distance between each pair of atoms and normalised an ideal gas of equal density. A more significant association is shown by a smaller interatomic gap (r) and a higher peak of g(r) [24, 25]. The equation below describes the RDF:

$$g_{xy}(r) = \frac{\langle Ny(r, r+dr) \rangle}{\rho_y 4\pi r^2 dr}$$

where ρ_y is the y atom's density, kg/m^3; r is s circular radius, Å; N_y is the number of y atoms or molecules [26].

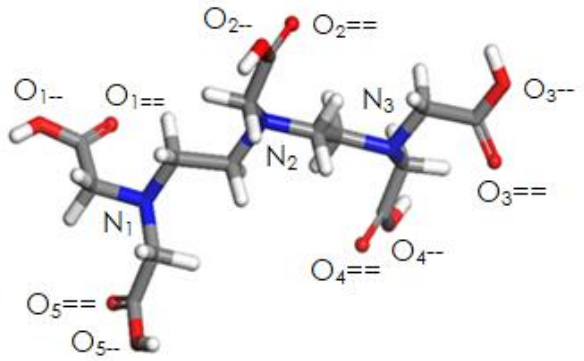

(a)

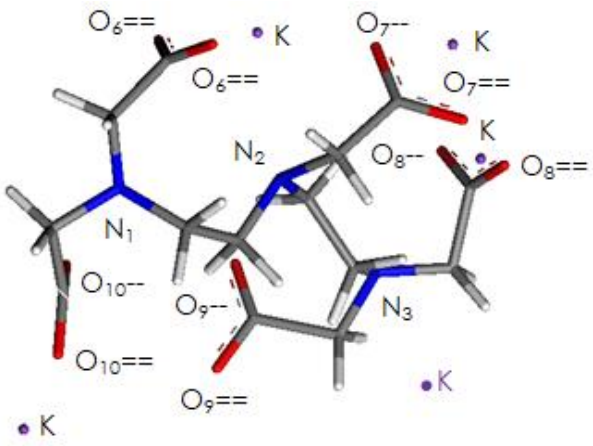

(b)

(c)

Figure 1 Atomic labelling of chemical structure for (a) diethylenetriaminepentaacetic acid (DTPA), (b) potassium salt diethylenetriaminepentaacetic acid (DTPA-K_5), and (c) calcium carbonate ($CaCO_3$). Colour representation: white – hydrogen, red – oxygen, blue – nitrogen, grey – carbon, purple – potassium and green – calcium

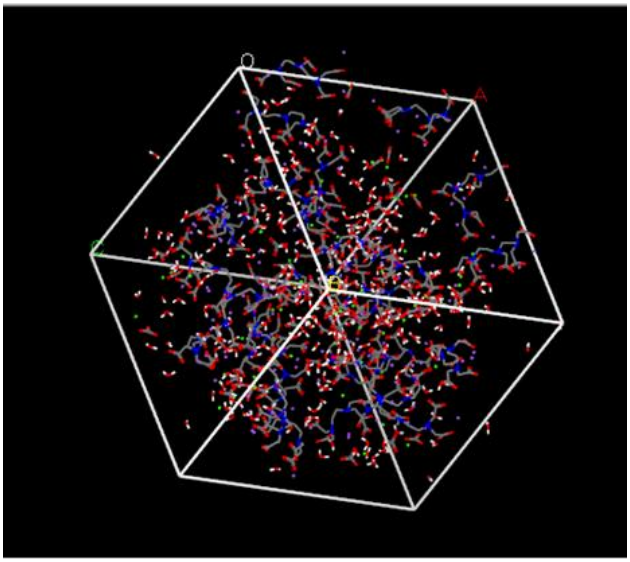

Figure 2 A cubical simulation model comprised of DTPA-K_5, $CaCO_3$ and water system

Table 1 Simulation parameter details for the DTPA and DTPA-K_5 system

	Number of molecules			
	DTPA	**DTPA-K_5**	**$CaCO_3$**	**Water**
System 1	30	-	-	270
System 2	30	-	60	270
System 3	-	30	-	270
System 4	-	30	60	270

3.0 RESULTS AND DISCUSSION

3.1 Intermolecular Interaction of DTPA and DTPA-K5 with H_2O molecules

The radial distribution function (RDF) is a normalisation form of atomic pair distribution function. Each reference atom x is measured the distance from every atom y. [27]. A study conducted to understand the early nucleation of crystallisation of solid from the solution used Lennard-Jones parameters. Solute-solute parameters characterised the solid phase and solvent–solvent characterised the liquid phase. The solvent-solute interaction was modified using Lorentz-Berthelot mixing rules [28]. In this work, the Lennard Jones was also selected to represent the van der Waals interaction in the solvent-solvent and solvent-solute interactions study. Figure 3 illustrates the RDFs plot of the hydrogen and oxygen of water in a DTPA molecule interaction. The first highest point was spotted at a radial distance, r, 1.75 Å between O--H_2O and H--DTPA interaction. The H_5--DTPA describes the most substantial interaction with the g(r) of 1.92 and H_3 at 1.27. The RDFs for H_3 increased at a distance of 4.25 Å and started to decline at 9.25 Å. At a distance beyond 9.25 Å, the intensity equals 0.92, indicating no long-range order interaction.

Meanwhile, the second peak shows the interaction between H--H_2O and O--DTPA occurs at a low probability with a radial distance, r, of 3.25 Å. A wide top curve with less intensity shows that H-H_2O and O_5--DTPA interaction with 1.08 g(r) occurs. In DTPA, the carboxylic group situated farthest from the amine group has the greatest contact as the intramolecular hydrogen bonding less impacts it between the central nitrogen and terminal acetate [29, 30, 31]. Overall, the intermolecular interactions at 60°C are considered strong, signifying that the solubility of DTPA solubility increased at higher temperatures but is minimal in water at room temperature.

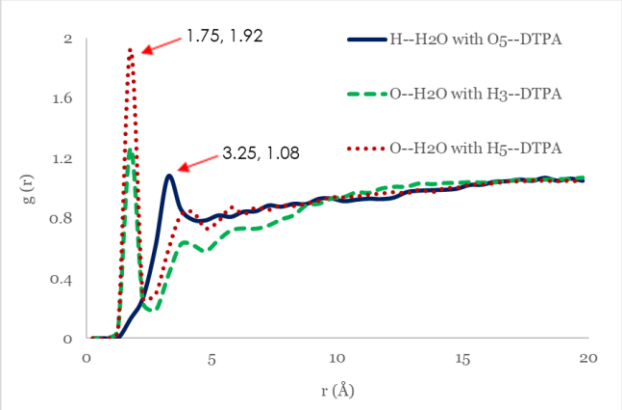

Figure 3 The g(r) plot for water showing molecular interactions between water (oxygen and hydrogen atoms) in DTPA carboxylic groups

The intermolecular interaction of water (oxygen and hydrogen atoms) with the DTPA-K_5 carboxylic groups is depicted in Figure 4. At a radius distance, r, 1.75 Å, the highest intermolecular interaction is O_{10}--H_2O, with the g(r) value of 1.57. By comparison, even though it has a low intensity, this intermolecular interaction occurs at a shorter distance than the interaction in DTPA, which is at 3.25 Å and g(r) 1.08 for the carboxylic group outermost from the amine.
In DTPA-K_5, the interactions between potassium and oxygen in water occur at a radius distance, r, 2.75 Å, with a value of 2.53 by g(r). The association of potassium and water leads to DTPA-K_5 being more excellent water solubility for stronger metal ion chelation [32]. Deprotonation of the DTPA occurs when all the protons have been captured. A strong metal hydroxide will sustain a high pH as the eight active ionic species of the DTPA ligands are charged negatively and improve the chelation capability [33]. Recently, among the top effective barium sulphate dissolution formulations are completely neutralised penta-potassium DTPA solutions with a pH greater than 12 [34]. In another modelling study, the DTPA with potassium carbonate, K_2CO_3 at high pH in the addition of KOH was suggested to eradicate different iron sulfide scale types such as $K_4Fe(II)_4(S_2H)_{12}$ and $K_3Fe(II)(S_2H)_5$ clusters. The dissolution of iron sulphide scale with DTPA under basic conditions is thermodynamically favoured [35, 36]. Therefore, it is suggested that the pH factor should be considered in future modelling work to understand at the molecule level the role of H^+ and OH^- in the chelation process of a solid scale such as calcium carbonate.

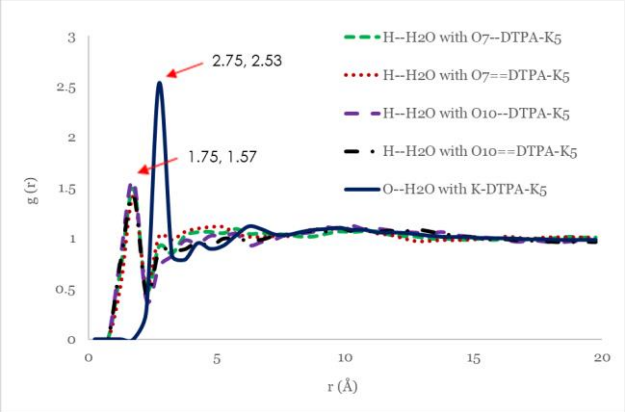

Figure 4 RDF plot between oxygen atoms in DTPA-K_5 molecule with water molecules

3.2 Intermolecular Interaction of DTPA and DTPA-K_5 with H_2O in the presence of $CaCO_3$

This section outlines the results analysis of the intermolecular interaction of DTPA with water in the existence of the $CaCO_3$ scale. Figure 5 illustrates a sharp RDFs pattern of O-H_2O with H_5–DTPA at a radial distance, r, 1.75 Å with g(r) of 0.81. It shows a declining value of g(r) compared to Figure 3, which at g(r) 1.92 in water. The RDFs began to rise at a distance of 3.25 and decrease at 4.00. At distances greater than 4.00, the intensity equals 1.00, suggesting no long-range order exists. Electrostatic interaction represents long-range interaction and van der Waals represents the short-range interaction between H_2O, DTPA and DTPA-K_5. Both interactions are non-bonded interactions. For example, Van der Waals forces are essential for the adsorption of isooctane and ethanol on a bcc Fe (100) surface. The polarizability of the molecules and the charge density distribution around the functional group affected the adsorption process [37]. The force is quantum mechanical in origin and arises from electrostatic interactions between fluctuations in the electronic charge density [38].

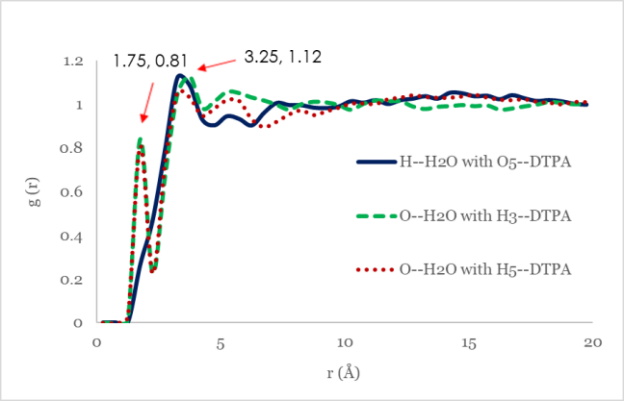

Figure 5 Interactions between DTPA carboxylic groups with a water molecule in the presence of $CaCO_3$

Figure 6 denotes a molecular interaction of DTPA-K_5 with water in existing $CaCO_3$. At a radius, r, 1.75 Å, O_{10}-- interaction was decreased from g(r) 1.57 to 1.21. A sharp peak of interaction between K--DTPA-K_5 and O--H_2O in $CaCO_3$ appears at a radius, r, of 2.75 Å. This demonstrates a strong intensity interaction of DTPA-K_5 in water, leading to enhanced solubility and dissolution property of DTPA-K_5 in water. This is one of the requirements of the chemical dissolver or chelating chemical, which needs to dissolve in water in the actual oil well operation.

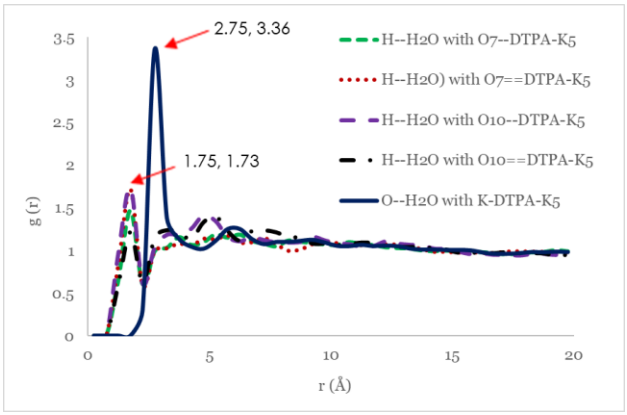

Figure 6 Water-oxygen intermolecular interaction in DTPA-K_5 carboxylate ions with the presence of $CaCO_3$

The strength of interaction between water and DTPA and water and DTPA-K_5 was not changed on the RDF values but the probability of occurring is less based on the reduced value of g(r) in Figures 5 and 6. The presence of the $CaCO_3$ scale reflects the molecular interaction formed between the chemical chelate and the $CaCO_3$ scale.

3.3 Intermolecular Interaction of DTPA and DTPA-K_5 with $CaCO_3$ (Metal Ion Complex)

This section explains the DTPA carboxylic group results in $CaCO_3$ solid scale dissolution. It represents the interactions of metal ion complexes. Both O_3 and O_5 are from hydroxyl group from DTPA. Figure 7 shows that the carbonyl groups have a more vital intensity interaction with calcium, as the first point or first neighbour atom is reflected at a radius, r, of 2.25 Å with an amount of g(r) 1.25 for O_3==Ca interaction. Meanwhile, the hydroxyl group shows a broad peak and low intensity at a radius, r, 4.25 Å, 1.79 for O_3--Ca interaction. Although the interactions at r = 2.25 Å are not as strong as of O-H_2O and H_5–DTPA (between water and DTPA) at the first neighbour radial distance of r = 1.75, the hydroxyl group in DTPA are abundant which would be an advantage in the formation of H-Bond metal either as a hydrogen donor and acceptor. The entire hydroxyl group deprotonated by forming a carboxylate ion in the chelation event [COO-]. This complexing signifies that the further delocalisation of electrons along

molecules of ligands and the metal ion is linked more closely [39].

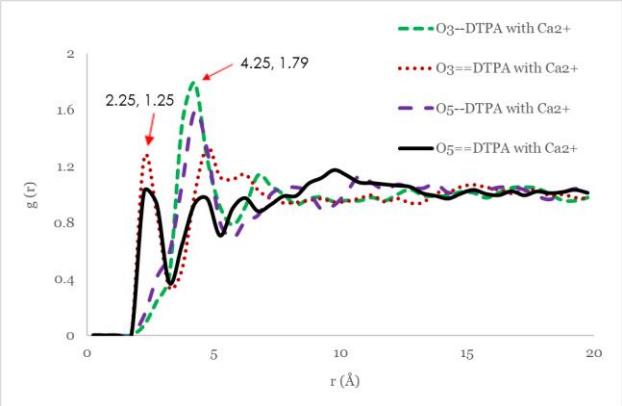

Figure 7 The g(r) plot intermolecular interactions of calcium ion complexes with the DTPA carboxylic group (hydroxyl and carbonyl)

Figure 8 illustrates the interactions of metal ion complexes by depicting the RDFs of DTPA-K_5 molecules with selected atoms in metal ions. The DTPA-K_5 molecule's oxygen atom binds significantly with calcium. The RDF of O_7==Ca exhibits a sharp peak with a higher intensity g(r) of 10.09 at a radius of 2.25 Å. These findings suggest that the O_7==Ca intermolecular interaction between $CaCO_3$ and DTPA-K_5 is strong. Thus, carboxylic groups in DTPA structure contribute the higher probability g(r) for intermolecular interaction of hydrogen bonding at a range of 2.25 - 2.45 Å between calcium.

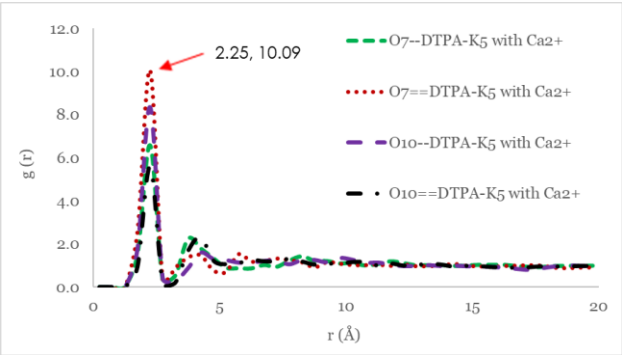

Figure 8 The g(r) plot intermolecular interactions of calcium ion complexes with the DTPA-K_5 carboxylic group (hydroxyl and carbonyl)

3.4 Intermolecular Interaction of amine in DTPA and DTPA-K_5 with $CaCO_3$

Figure 9 illustrates the RDF trend for intermolecular interaction between the amine functional group of DTPA and DTPA-K_5 with calcium carbonate, $CaCO_3$. The two amines, N_1 and N_3, association in DTPA exists with g(r) of 1.14 for calcium at 5.75 Å. The findings of simulations reflect the low degree of intensity and are presumably induced by intermolecular hydrogen bonding. For DTPA-K_5, the interaction of calcium arises at r, 2.25 Å with an intensity of 2.51 in N_1. This value has also supported the finding whereby the bond interaction between Ca-N is in the range of 2.38 to 2.66 Å [40]. The amine group is situated at the molecule core, while the carbonyl groups act as an arm, which provides a facility to capture metal ions during chelation. Mefenamic acid solute demonstrated high solubility values in dipolar aprotic solvents, followed by polar protic solvents and low solubility in a polar a protic solvent. Different hydrogen bonding propensities in the solvents contributed to different solubility values [41]. Thus, the carboxylic group in DTPA is important to form the van der Waals interaction, such as hydrogen bonding between the water and $CaCO_3$ scale in the presence of calcium.

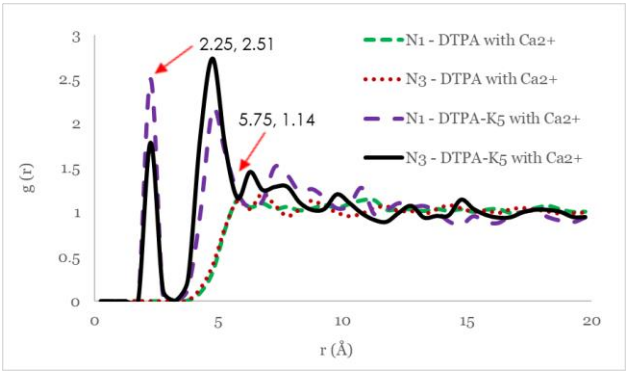

Figure 9 The g(r) plot intermolecular interactions between amine in DTPA and DTPA-K_5 with calcium

4.0 CONCLUSION

This work has successfully gained an insight into the molecular interaction of DTPA and DTPA-K_5 with $CaCO_3$. The simulation results showed the hydrogen bonding occurs between DTPA in water. Meanwhile, RDF for hydroxyl and carbonyl of the DTPA-K_5 carboxylic group significantly affects calcium ions in the chelation process with sharp peak of interaction at 2.25 Å and higher intensity of g(r). Without K in DTPA structure, the RDF trends demonstrated the poor interaction between amines and calcium.

Acknowledgement

The authors would like to thank Universiti Malaysia Pahang for research grants funding (RDU 170323 and PGRS 180394) and Setegap Ventures Petroleum Sdn. Bhd. for technical assistance, which contributed to the work designated here.

References

[1] Khan, W., Azari, M., Hamza, F., Hadibeik, H., and Ramakrishna, S. 2017. Case Study: Multirate Multizone Production Logging and Testing Provides Real-Time Reservoir Insight for Stimulation Treatment Optimization in Deepwater GOM. *SPE Annual Technical Conference and Exhibition*. San Antonio, Texas, USA. 9-11 October 2017. 1-15.
DOI: https://doi.org/10.2118/187407-MS.

[2] Olajire, A. A. 2015. A Review of Oilfield Scale Management Technology for Oil and Gas Production. *Journal of Petroleum Science and Engineering*. 135: 723-737.
DOI: https://doi.org/10.1016/j.petrol.2015.09.011.

[3] Dixon, N. J. 2012. *Handbook of Green Chemistry*. First published. Wiley-VCH Verlag GmbH & Co. KGaA.
DOI: https://doi.org/10.1002/9783527628698.hgc104.

[4] Li, N., He, D., Zhao, L., and Liu, P. 2016. An Alkaline Barium and Strontium-Sulfate Scale Dissolver. *Chemistry and Technology of Fuels and Oils*. 52: 141-148.
DOI: https://doi.org/10.1007/s10553-016-0684-3.

[5] Hassan, A., Mahmoud, M., Bageri, B. S., Aljawad, M. S., Kamal, M. S., Barri, A. A., and Hussein, I. A. 2020. Applications of Chelating Agents in the Upstream Oil and Gas Industry: A Review. *Energy & Fuels*. 34(12): 15593-15613.
DOI: https://doi.org/10.1021/acs.energyfuels.0c03279.

[6] Wang, K. S., Resch, R., Dunn, K., Shuler, P., Tang, Y., Koel, B. E., and Fu Yen, T. 1999. Dissolution of the Barite (001) Surface by the Chelating Agent DTPA as Studied with Non-Contact Atomic Force Microscopy. *Colloids and Surfaces A: Physicochemical and Engineering Aspects*. 160(3): 217-227.
DOI: https://doi.org/10.1016/S0927-7757(99)00183-1.

[7] Nasr-El-Din, H. A., Al-Mutairi, S. H., Al-Hajji, H. H., and Lynn, J. D. 2004. Evaluation of a New Barite Dissolver: Lab Studies. *SPE International Symposium and Exhibition on Formation Damage Control*. Lafayette, Louisiana. 18-20 February 2004. 1-11.
DOI: https://doi.org/10.2118/86501-MS.

[8] Gamal, H., Al-Afnan, S., Elkatatny, S., and Bahgat, M. 2021. Barium Sulfate Scale Removal at Low-Temperature. *Geofluids*. 2021: 1-12.
DOI: https://doi.org/10.1155/2021/5527818.

[9] Abib, G. A. P., Cruz, G. F. D., Vaz Junior, A. S. L. 2018. Study of Barium Sulfate Dissolution by Scale Dissolver Based on Solutions of DTPA. *Anais da Academia Brasileira de Ciências*. (3): 3185-3196.
DOI: https://doi.org/10.1590/0001-3765201820170728.

[10] Khaled, A., Mohamed, M., Salaheldin, E., and Patil, S. 2019. Effect of Calcium Carbonate on Barite Solubility Using a Chelating Agent and Converter. *SPE International Conference on Oilfield Chemistry*, Galveston, Texas, USA, April 2019. 1-10.
DOI: https://doi.org/10.2118/193566-MS.

[11] Sulaiman, M. H., Adam, F., Yaacob, Z., Sujak, M. Z., and Mohd Noor, M. Z. 2020. Intermolecular Interaction of Carboxylic Group with Calcium Ions and Dissolution of Solid Scales in Bmim-PF6 and Tba-NfO ionic Liquid Solution. *Malaysian Journal of Microscopy*. 16(1): 205-216.

[12] Fredd, C. N and Fogler, H. S. 1997. Chelating Agents as Effective Matrix Stimulation Fluids for Carbonate Formations. *SPE International Symposium on Oilfield Chemistry*. Houston, Texas, USA, 18-21 February 1997.
DOI: https://doi.org/10.2118/37212-MS.

[13] Almubarak, T., Ng, J. H., and Nasr-El-Din, H. 2017. Chelating Agents in Productivity Enhancement: A Review. *SPE Oklahoma City Oil and Gas Symposium*. Oklahoma City. USA. 27-31 March 2017.
DOI: https://doi.org/10.2118/185097-MS.

[14] Ramanathan, R., and Nasr-El-Din, H. 2019. Evaluation of Chelating Agents for Iron Sulfide FeS Scale Removal. *SPE Abu Dhabi International Petroleum Exhibition and Conference*. Abu Dhabi, UAE. 11-14 November 2019.
DOI: https://doi.org/10.2118/197891-MS.

[15] Sulaiman, M. H., Adam, F., Yaacob, Z., and Mohd Noor, M.Z. 2020. Synthesis of Ionic Salt for Calcite and Barite Solid Scale Dissolution. *IOP Conference Series: Materials Science and Engineering*. 736: 1-7.

[16] Sulaiman, M. H., Adam, F., Yaacob, Z., Mohd Noor, M. Z., and Abdullah, N. 2022. Evaluation of Carboxylic Acid and Amine Groups with $CaCO_3$, FeS and $BaSO_4$: Molecular Dynamic Simulations and Experimental Study. *Arabian Journal for Science and Engineering*.
DOI: https://doi.org/10.1007/s13369-022-06647-2.

[17] Adam, F., Abu Bakar, S. H., Mohd Yusoff, M., and Tajuddin, S. N. 2014. Molecular Dynamic Simulation of the Patchouli Oil Extraction Process. *Journal of Chemical & Engineering Data*. 59(2): 183-188.
DOI: https://doi.org/10.1021/je3013292.

[18] Abdul Mudalip, S. K., Adam, F., and Abu Bakar, M. R. 2019. Evaluation of the Intermolecular Interactions and Polymorphism of Mefenamic Acid Crystals in N,N-Dimethyl Formamide Solution: A Molecular Dynamics Simulation and Experimental Study. *Comptes Rendus Chimie*. 22(11-12): 771-778.
DOI: https://doi.org/10.1016/j.crci.2019.08.005.

[19] Van Gunsteren, W. F., and Berendsen, H. J. C. 1990. Computer Simulation of Molecular Dynamics: Methodology, Applications, and Perspectives in Chemistry. *Angewandte Chemie International Edition in English*. 29(9): 992-1023.
DOI: https://doi.org/10.1002/anie.199009921.

[20] Rigby, D. 2004. Fluid Density Predictions using the COMPASS Force Field. *Fluid Phase Equilibria*. 217(1): 77-87.
DOI: https://doi.org/10.1016/j.fluid.2003.08.019.

[21] Sun, H. 1998. COMPASS: An ab Initio Force-Field Optimised for Condensed-Phase Applications Overview with Details on Alkane and Benzene Compounds. *The Journal of Physical Chemistry B*. 102(38): 7338-7364.
DOI: https://doi.org/10.1021/jp980939v.

[22] Sun, H., Ren, P., and Fried, J. R. 1998. The COMPASS Force Field: Parameterisation and Validation for Phosphazenes. *Computational and Theoretical Polymer Science*. 8(1-2): 229-246.
DOI: https://doi.org/10.1016/S1089-3156(98)00042-7.

[23] Yang, X., Feng, Y., Jin, J., Liu, Y., and Cao, B. 2019. Molecular Dynamics Simulation and Theoretical Study on Heat Capacities of Supercritical H_2O/CO_2 Mixtures. *Journal of Molecular Liquids*. 299: 1-10.
DOI: https://doi.org/10.1016/j.molliq.2019.112133.

[24] Yu, X., Wu, Y., Wang, J., and Ulrich, J. 2018. Experimental Assessment and Modeling of the Solubility of Malonic Acid in Different Solvents. *Chemical Engineering and Technology*. 41(6): 1098-1107.
DOI: https://doi.org/10.1002/ceat.201700227.

[25] Leach, A. R. 2001. Computer Simulation Methods. *Molecular Modelling: Principles and Applications*. Second Edition. Prentice Hall.

[26] Hamad, S., Moon, C., A. Catlow, C. R., T. Hulme, A., and L. Price, S. 2006. Kinetic Insights into the Role of the Solvent in the Polymorphism of 5-Fluorouracil from Molecular Dynamics Simulations. *Journal of Physical Chemistry B*. 110(7): 3323-3329.
DOI: https://doi.org/10.1021/jp055982e.

[27] Terban, M. W., and Billinge, S. J. L. 2022. Structural Analysis of Molecular Materials Using the Pair Distribution Function. *Chemical Reviews*. 122(1): 1208-1272.
DOI: https://doi.org/10.1021/acs.chemrev.1c00237.

[28] Anwar, J., & Boateng, P. K. 1998. Computer Simulation of Crystallization from Solution. *Journal of the American Chemical Society*. 120(37): 9600-9604.
DOI: https://doi.org/10.1021/JA972750N.

[29] Sandoval, A. A., Sandoval, M. W., Lin, E., and Cheng, K. L. 1969. Hydrogen Bonding in Some Polyaminocarboxylic Acids. *Journal of Magnetic Resonance*. 3(2): 258-268.

DOI: https://doi.org/10.1016/0022-2364(70)90052-1.
[30] Ladd, M. F. C., Povey, D. C., and Stace, B. C. 1974. Crystallographic and Spectroscopic Studies on Ethylenediaminetetraacetic Acid (edta) III. Crystal and Molecular Structure of a-edta and Infrared Studies on a- and β-edta. *Journal of Crystal and Molecular Structure*. 4: 313-325.
DOI: https://doi.org/10.1007/BF01636045.
[31] Kowacz, M., Putnis, C. V., and Putnis, A. 2009. The Control of Solution Composition on Ligand-Promoted Dissolution: DTPA−Barite Interactions. *Crystal Growth & Design*. 9(12): 5266-5272.
DOI: https://doi.org/10.1021/cg9007894.
[32] Kamal, M. S., Hussein, I., Mahmoud, M., Sultan, A. S., and Saad, M. A. S. 2018. Oilfield Scale Formation and Chemical Removal: A Review. *Journal of Petroleum Science and Engineering*. 171: 127-139.
DOI: https://doi.org/10.1016/j.petrol.2018.07.037.
[33] Luo, Z., Zhang, N., Wang, C., Wu, L., Liu, P., and Ji, H. 2020. A Chelating Agent System for the Removal of Barium Sulfate Scale. *Journal of Petroleum Exploration and Production Technology*. 10: 3069-3079.
DOI: https://doi.org/10.1007/s13202-020-00886-5.
[34] Hassan, A., Mahmoud, M., Bageri, B. S., Aljawad, M. S., Kamal, M. S., Barri, A. A., and Hussein, I. A. 2020. Applications of Chelating Agents in the Upstream Oil and Gas Industry: A Review. *Energy & Fuels*. 34(12): 15593-15613.
DOI: https://doi.org/10.1021/acs.energyfuels.0c03279.
[35] Buijs, W., Hussein, I. A., Mahmoud, M., Onawole, A. T., Saad, M. A., and Berdiyorov, G. R. 2018. Molecular Modeling Study toward Development of H_2S-Free Removal of Iron Sulfide Scale from Oil and Gas Wells. *Industrial & Engineering Chemistry Research*. 57(31): 10095-10104.
DOI: https://doi.org/10.1021/acs.iecr.8b01928.
[36] Mahmoud, M., Hussein, I. A., Sultan, A., Saad, M. A., Buijs, W., and Vlugt, T. J. H. 2018. Development of Efficient Formulation for the Removal of Iron Sulphide Scale in Sour Production Wells. *The Canadian Journal of Chemical Engineering*. 96(12): 2526-2533.
DOI: https://doi.org/10.1002/cjce.23241.
[37] Bedolla, P. O., Feldbauer, G., Wolloch, M., Eder, S. J., Dörr, N., Mohn, P., Redinger, J., and Vernes, A. 2014. Effects of van der Waals Interactions in the Adsorption of Isooctane and Ethanol on Fe(100) Surfaces. *The Journal of Physical Chemistry C*. 118(31): 17608-17615
DOI: https://doi.org/10.1021/jp503829c.
[38] Hermann, J., Jr, R. A. D., and Tkatchenko, A. 2017. First-Principles Models for van der Waals Interactions in Molecules and Materials: Concepts, Theory, and Applications. *Chemical Reviews*. 117(6): 4714-4758
DOI: https://doi.org/10.1021/acs.chemrev.6b00446.
[39] Onawole, A. T., Hussein, I. A., Saad, M. A., Mahmoud, M., Ahmed, M. E. M., and Nimir, H. I. 2019. Effect of pH on Acidic and Basic Chelating Agents Used in The Removal of Iron Sulfide Scales: A *Computational Study*. 178: 649-654.
DOI: https://doi.org/10.1016/j.petrol.2019.03.075.
[40] Gerig, J. T., Singh, P., Levy, L. A., and London, R. E. 1987. Calcium Complexation with a Highly Calcium Selective Chelator: Crystal Structure of Ca(CaFBAPTA)·$5H_2O$. *Journal of Inorganic Biochemistry*. 31(2): 113-121.
DOI: https://doi.org/10.1016/0162-0134(87)80056-9.
[41] Mudalip, S. K., Abu Bakar, M. R., Jamal, P., and Adam F. 2013. Solubility and Dissolution Thermodynamic Data of Mefenamic Acid Crystals in Different Classes of Organic Solvents. *Journal of Chemical & Engineering Data*. 58(12): 3447-3452.
DOI: https://doi.org/10.1021/je400714f.